Optimized Digital Webcam with Hungry Roach Infestation Optimization to Monitor the Drying Process of Cassava Chips

Yusuf Hendrawan[1], La Choviya Hawa[1], Retno Damayanti[1], Dimas Firmanda Al Riza[1], Mochamad Bagus Hermanto[1], and Sandra Malin Sutan[1]

[1] *Department of Biosystem Engineering, Universitas Brawijaya, Jl. Veteran Malang, ZIP 65145, Indonesia*

yusuf_h@ub.ac.id

Abstract. This study utilizes Logitec HD webcam C270 as a computer vison-based precision monitoring system to optimize the performance of cassava chips drying machines. Cassava chips processed from optimal drying is later utilized as raw material for quality modified cassava flour (MOCAF). The purpose of this study is to optimize the selection of textural features (TFs) in computer vision to predict the water content of cassava chips during the drying process by applying a combination of optimization methods, commonly referred as hungry roach infestation optimization (HRIO) algorithm and modeling methods, which is artificial neural network (ANN). Multi-objective optimization (MOO) was performed with two objectives, by maximizing the accuracy of the predicted water content of cassava chips and by minimizing the number of feature subset of a total of 260 TFs. The test results indicate that the best feature subset depict the 6 TFs such as grey energy, hue energy, red entropy, saturation$_{(HSV)}$ contrast, green homogeneity, and grey correlation. The best feature subset has been tested as ANN input to predict the water content of cassava chips during the drying process (presenting the expected results), marked with the achievement of R^2 values between real data and predictive data of 0.98. The results of the measurement of mean square error (MSE) on the training data are 0.000056 and the MSE value in the validation data of 0.000098.

Keywords: Cassava chips, computer vision, drying process.

1 Introduction

Cassava products (*Manihot escullenta Crantz*) have been commonly processed into food (edible) products, such as: fermented, steamed, fried cassava, and flour as the raw

Q. D. Utama et al. (eds.), *Proceedings of the 7th International Conference on Food, Agriculture, and Natural Resources (IC-FANRES 2022)*, Advances in Biological Sciences Research 35,
https://doi.org/10.2991/978-94-6463-274-3_22

ingredient for cake or bread making. There are two types of flour made from cassava, which are cassava starch and cassava flour [1]. Cassava flour has an advantage over tapioca flour (which only uses cassava starch) containing protein, fat, calcium, phosphorus and iron. However, another disadvantage of processing cassava starch is the high nitrogen content, resulting a brownish color when heated during the drying process [2]. To overcome this, a refinement process is carried out to modify the processing of cassava starch, commonly referred as modified cassava flour (MOCAF). The development of the diversification of cassava into MOCAF provides a promising attempt to substitute the utilization of wheat flour [3].

In general, the drying process becomes a very important stage in handling agricultural products [4]. This process is also included in the process of making flour, to determine the quality of the produced flour [5]. Drying is a process to reduce the water content in an agricultural material; thus, the end result is expected to contain with optimal water content as the subsequent. Drying also aims to increase the shelf life of food products [6]. Drying is the process of heat and material mass transfer [7]. The process of transferring heat occurs through a conduction process, where heat is transferred into the material by transferring heat by conduction reaction. The water content in the material comes out and evaporates causing the displacement of the material. Drying method is suggested in processing food products by utilizing artificial drying due to its numerous advantages [8]. Such advantages occur in artificial drying as the process involves controlling temperature and air velocity to be optimally adjusted to produce a drying process (faster, randomly, hygienically, and able to maintain the nutritional content of food products). One example of an artificial drying tool is a rack-type drying machine [9], working with the help of heat which can be optimally adjusted and easily operated. The shelves in the drying machine provide holes for the channel to distribute hot air to the material. The process of distributing hot air to the material will cause the loss of water content in the dried material to run optimally.

The expected quality of cassava chips determines the quality of the process of making cassava starch at MOCAF. To determine the quality of cassava chips, it is necessary to test physical and chemical characteristics by performing the conventional tests requiring laboratory work with a considerable amount of time. In the drying process, several problems often arise, such as the difficulty of controlling temperature and humidity, the presence of microbial contamination, and also the dependence on local weather conditions.

Aghbashlo *et al.* [10] employed the computer vision method to monitor the quality of food products during the real-time drying process. This method is proven to be suitable for observing changes in food products during drying process for revealing the mechanical, sensory, and nutritional characteristics. The computer vision method that has been developed includes real-time monitoring in terms of shape, size, color, and texture. With various advantages of computer vision, this method can be further developed for online and real-time monitoring processes to regulate various control parameters to produce desired products. With the existence of a monitoring system, setting the characteristics of drying products can be evaluated during the drying process to meet the expected standards. Dutta *et al.* [11] applied computer vision as a non-destructive sensing method to identify the presence of acrylamide in potato chips. The first step in image processing involves the automatic separation of potato chips from the background, which is then followed by extraction of statistical data and textural features

(TFs) of the previously separated object image. The results indicate a high level of accuracy of more than 94%. Baigvand *et al.* [12] examined the application of computer vision for the grading process with the dried fig objects. The results indicate an accuracy of more than 95.2%. Benalia *et al.* [13] developed an automatic system based on computer vision to improve the quality of system control in sorting the dried figs objects. In this study, a color space model was utilized including CIE XYZ, CIE Lab, and Hunter Lab. The model was utilized to measure the browning index of each fruit with accuracy of 99.5%. Romani *et al.* [14] applied computer vision to analyze digital images especially in the external visual appearance of potato chips products during the frying process. The result indicates a high correlation with of $R^2 > 0.962$ by applying computer vision (RGB color) with conventional tools (colorimeter) to evaluate the physical properties of potato chips during the frying process. Yadollahinia and Jahangiri [15] developed thin-layer dryer devices with computer vision applications employing image analysis software to monitor the drying process of cut potato products. The results present that computer vision systems have been successful in monitoring the period of shrinkage that occurs in cut potatoes during the drying process.

In the field of agriculture and biological engineering, most researchers have developed various intelligent modeling methods such as artificial neural network (ANN) to analyze various food processing [16]. Khazaei *et al.* [17] examined the modeling method for predicting the drying process in grapes with system control and online monitoring. Computer vision is employed to measure weight shrinkage in grapes during the drying process for the production of raisins. ANN was developed as an intelligent modeling method to model the drying process of grapes by utilizing a hot air dryer. The best ANN model is obtained by using a three-layer structure with R^2 value of 0.99947 for training data and R^2 of 0.99952 for testing data. For the food quality control sector, ANN has been proven to be successfully implemented to predict the quality of agricultural raw products [18-20]. Azadbakht *et al.* [21] examined the application of ANN for energy analysis in fluidized bed dryers for cut-potato products. The results of the statistical analysis demonstrate that ANN is applicable for drying process to model energy use in the food industry. Wu *et al.* [22] have successfully developed the latest intelligent control system based on analysis of digital images of tobacco leaves in real-time mode to monitor the physical characteristics of tobacco leaves applying an ANN model.

ANN modeling performance can be improved by adding an input parameter selection process. The selection of suitable input parameters will result in ANN modeling with better accuracy, commonly recognized as feature selection. Principally, feature selection method selects optimal feature subset that can maximize the prediction accuracy of ANN. Irrelevant features demonstrate high performance when combined with other features [23]. Several previous studies have proven the advantages of utilizing natural-inspired algorithms as a feature selection method [24-28]. Hendrawan and Al Riza [29] have successfully implemented the hungry roach infestation optimization (HRIO) method to select features as ANN inputs to predict the water content of biological objects. The results of the research developed by Hendrawan and Murase [28] also demonstrate the superiority of the HRIO method compared to other optimization methods such as genetic algorithms, discrete particle swarm optimization, dan simulated annealing.

The conventional method through direct measurement of the moisture content in the material (during the drying process) is required to compare the models with the

computer vision method. The principle of monitoring on the drying machine control system is to stop the drying process when the water content of the material has reached the desired optimum point. The application of computer vision technology has been successful and developed in various fields of food products for inspection, classification, and product evaluation. Therefore, the purpose of this study is to model the image feature to predict the water content of cassava chips during the drying process by employing ANN modeling and to optimize the selection process for achieving the best image feature-subset by HRIO.

2 Materials and Methods

Cassava was obtained directly from one farm in the area of Malang, East Java, Indonesia. Five hundred samples of cassava chips with various moisture content conditions were utilized in this study. As a method for manipulating physiological conditions, each sample of cassava chips was regulated by its water content through various durations of drying. The moisture content of a material can be defined as the percentage of water contained in the sample material from its initial weight [30]. The drying experiment was carried out using tray dryer as illustrated in Figure 1, where the dryer can be controlled in a temperature range between 50-70 ºC. Before the study began, cassava was washed, peeled and thinly cut into 1 mm thickness chips by using a mechanical slicing machine.

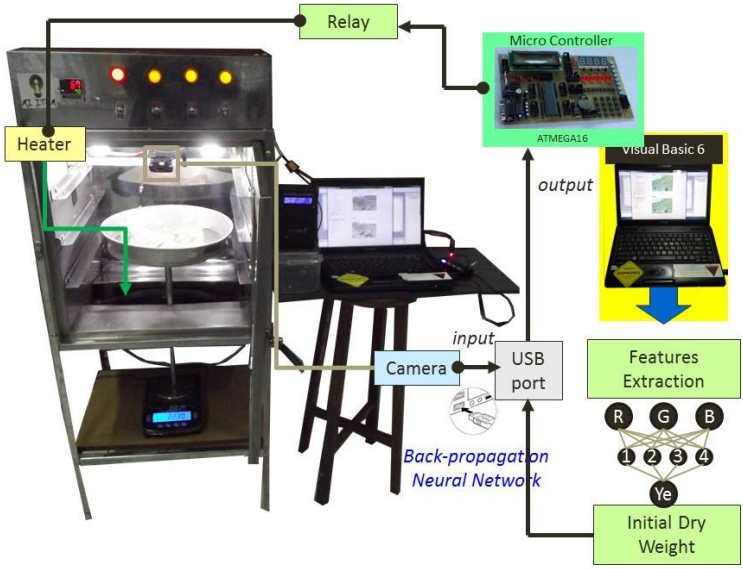

Fig. 1. Modified cassava chips tray dryer using computer vision and ANN.

The first stage of the research was conducted by performing digital image capture, where images of cassava chips were seized by a digital camera (Logitec HD Webcam C270, Japan) and were placed at an altitude of 300 mm from the surface of the material and were connected directly via USB port on a central computer by using an Intel core i7 processor. Digital cameras used for digital image processing provided a choice of

image formats in the form of BMP. Digital images were captured by using the optimal resolution of 1280 × 720 and were stored on the computer via USB port in BMP format. Uniform lighting conditions on all object surfaces become important factors in computer vision [31] to optimally control the light distribution. The lighting source commonly employs the two 22W lamps (EFD25N / 22. National Corporation, Japan). The light intensity on the surface of the cassava chips object is controlled to be uniform at a value of 300 lux during the digital image capture process. During the drying process, the digital image of cassava chips is carried out continuously using self-built computer vision software. During the drying process until the weight of cassava chips reaching a constant condition, the lost water weight on cassava chips objects is measured by using digital scales every one minute. At the same time, digital shooting is also performed in every one minute. After the drying process is completed, 500 image data with various water content statuses (range 1 = wet; range 2 = semi-dry; and range 3 = optimum dry) are prepared for the next process of image analysis with software specifically built by Visual Basic 6.0 to observe the water content of cassava chips. Image parameters measured by this software are TFs for each digital image data.

After the data from the image analysis is obtained, the next step to perform is modeling. Data modeling in this study applies back-propagation neural network (BPNN) to model TFs as input with cassava chips water content as output. Supervised prediction is utilized to predict the water content of cassava chips by using digital image parameters. This research is related to the measurement of the optimal dryness level of cassava chips during the drying process by comparing two analytical methods of image analysis and conventional measurement of moisture content. The next step is continued to optimize the image parameters as modeling inputs. The optimization process is related to the feature selection process to select the most accurate combination of image parameters to predict the water content of cassava chips. The feature selection method employs a nature-inspired algorithm approach (HRIO method). Multi objective optimization (MOO) utilized in this study includes two optimization objectives for minimizing the value of mean square error (MSE) and minimizing the number of feature subset [32]. Thus, the formula for the fitness value used is as follows:

$$function_1 = weight_1 \times MSE_{(x)} \tag{1}$$

$$function_2 = weight_2 \times \frac{IF_{(x)}}{f_t} \tag{2}$$

$$fitness(x) = function_1 + function_2 \tag{3}$$

where $MSE_{(x)}$ is the mean square error for validation data from BPNN using selected feature-subset x input; $IF_{(x)}$ is the number of image parameters selected in feature-subset x; f_t is the total number of overall image parameters; $weight_1$ and $weight_2$ are two priority weights related to the level of importance of the accuracy factor and the number of selected image parameters; where in this study, the accuracy factor is more important than the number of selected image parameters;thus, the value is set at $weight_1 = 0.6$ and $weight_2 = 0.4$ based on preliminary research.

Texture analysis can be considered as one of the reliable methods for extracting digital image parameters [33-34]. The procedure for calculating the color co-occurrence matrix (CCM) consists of three main stages, including: (1) digital images which are converted from RGB colors to other color representations such as grey [35], hue-

saturation-lightness (HSL), hue-saturation-value (HSV) [36], Lab, XYZ [37], LCH [38], LUV [39], CMY, and CMYK; (2) calculation of spatial gray-level dependence matrix (SGDM) [40], which produces one CCM for each color space, where the CCM value is built based on normalized color data values; and (3) calculation of ten formulas of Haralick TFs [27]. Ten Haralick TFs equations, is derived from a formula:

$$Energy = \sum_{i}^{M}\sum_{j}^{N} P^2[i,j] \tag{4}$$

$$Entropy = -\sum_{i}^{M}\sum_{j}^{N} P[i,j]\log P[i,j] \tag{5}$$

$$Contrast = \sum_{i}^{M}\sum_{j}^{N} (i-j)^2 P[i,j] \tag{6}$$

$$Homogeneity = \sum_{i}^{M}\sum_{j}^{N} \frac{P[i,j]}{1+|i-j|} \tag{7}$$

$$Inverse\ DifferenceMoment = \sum_{i}^{M}\sum_{j}^{N} \frac{P[i,j]}{|i-j|^k} \quad i \neq j \tag{8}$$

$$Correlation = \sum_{i}^{M}\sum_{j}^{N} \frac{(i-\mu)(j-\mu)P[i,j]}{\sigma^2} \tag{9}$$

$$Sum\ Mean = \frac{1}{2}\sum_{i}^{M}\sum_{j}^{N} (iP[i,j] + jP[i,j]) \tag{10}$$

$$Variance = \frac{1}{2}\sum_{i}^{M}\sum_{j}^{N} ((i-\mu)^2 P[i,j] + (j-\mu)^2 P[i,j]) \tag{11}$$

$$Cluster\ Tendency = \sum_{i}^{M}\sum_{j}^{N} (i+j-2\mu)^k P[i,j] \tag{12}$$

$$Maximum\ Probability = \max_{i,j}^{M,N} P[i,j] \tag{13}$$

where $P(i, j)$ is the element to $(i, j)^{th}$ of the normalized co-occurrence matrix value, while μ and σ are the average values and the standard deviation of the pixel element of the digital image is calculated by using the following equation:

$$P[i,j] = \frac{N(i,j)}{M} \tag{14}$$

$$\mu = \sum_{i}^{M} i \sum_{j}^{N} P[i,j] \tag{15}$$

$$\sigma = \sum_{i}^{M} (i-\mu)^2 \sum_{j}^{N} P[i,j] \tag{16}$$

wherein $N(i,j)$ is the number of normalized values of pixel pairs in digital images, constructed of values of pixel intensity to i and pixel intensity values to j, while M is the total number of pixels in digital images.

The results of preliminary studies using various combinations of variations in angle values ($\theta = 0^o$, $\theta = 45^o$, $\theta = 90^o$, $\theta = 135^o$) and distance values ($d = 1$, $d = 2$, $d = 3$)

indicate that angle combinations ($\theta = 0^o$) and distance ($d = 1$) has the best performance compared to the combination of θ and the other d to identify the water content in cassava chips. Therefore, in this study, TFs were calculated by using the best values of θ and d. As a result, the total number of TFs is 260 which includes 10 TFs for each color space of R, G, B, grey, hue, saturation$_{(HSL)}$, saturation$_{(HSV)}$, lightness$_{(HSL)}$, value$_{(HSV)}$, X$_{(XYZ)}$, Y$_{(XYZ)}$, Z$_{(XYZ)}$, L$_{(Lab)}$, a$_{(Lab)}$, b$_{(Lab)}$, C$_{(LCH)}$, H$_{(LCH)}$, u$_{(Luv)}$, v$_{(Luv)}$, C$_{(CMY)}$, M$_{(CMY)}$, Y$_{(CMY)}$, C$_{(CMYK)}$, M$_{(CMYK)}$, Y$_{(CMYK)}$, and K$_{(CMYK)}$.

The BPNN three-layer structure is applied in this study including input layer, one hidden layer, and output layer. The learning rate and momentum values are set with values of 0.1 and 0.9. The number of hidden nodes in the hidden layer is set to 20. The input in this study is the digital image parameter while the output is the cassava chips water content value. The performance of the training process and validation is determined by the predicted MSE value, as follows:

$$MSE = \frac{1}{N_n}\sum_{i=1}^{N_n}(S_i - St_i)^2 \tag{17}$$

where N_n is the amount of data used, S_i is the water content value of cassava chips predicted by using the BPNN model, and St_i is the real water content of cassava chips. A total of 500 data samples were randomized and divided into two parts of 400 data samples for training sets and 100 data samples for validation sets.

HRIO is inspired by the optimum behavior of cockroaches. There are three basic cockroach behaviors that can be referred as optimization techniques, which are [41]:

1. *Find_Darkness*: cockroach behavior to find the darkest shelter. The level of darkness in the search location can be compared as the fitness function at the optimum location $F(x)$.
2. *Find_Friends*: cockroach behavior to socialize with nearby cockroaches with stop probability values ($1 / \tau_{stop}$, N) per unit time when meeting as many as N, such as: 0.49 / s for $N = 1$, 0.63 / s for $N = 2$, and 0.65 / s for $N = 3$ [42]. If individual cockroaches are within the radius of another cockroach area, then there is a probability of $1 / \tau_{stop}$, N of cockroach individuals to socialize with other cockroaches. This socialization process is interpreted in the form of an algorithm to share information, where the information shared is the darkest location known by each individual cockroach or can be referred as a personal best solution (p). When two cockroachs meet, it is possible they will communicate with their neighbors (N) about the knowledge of the darkest location they have ever encountered. Thus, the location of the darkest location in the cockroach group can be defined as a local best solution (l).
3. *Find_Food*: cockroach behavior when hungry to look for food. Food locations are located randomly in the search area. This food-seeking behavior in optimization techniques aims to make the process of finding the optimum point untrapped in the local optima.

The stages in the HRIO algorithm for the feature selection depicted in Figure 2 are as follows [28]:

1. Initializing the HRIO parameters, the maximum iteration value is set to max = 500, and the number of cockroach populations is set to $N_a = 70$. Parameter neighbors are set as $A_1 = 0.49$, $A_2 = 0.63$ and $A_3 = 0.65$. The parameter hunger is set to t_{hunger} =

100. The probability value for mutation is set to $w = 0.5$. The probability crossover (C_o) value is set at a variable value in the sensitivity analysis process.

2. Determining the location of the cockroach (x_i) randomly with the value of $hunger_i$ = rand {0, t_{hunger}-1}. Each cockroach has a solution as a feature subset (x_i: 0,1,1,0,0,0,0,1,0,0,1,0, ...m), where m represents the total number of TFs (260 TFs). Each x_i in the population represents the candidate solution to the problem of feature subset selection. A value of 0 indicates that the TFs are not selected, and are not included as BPNN input, while value of 1 means that the TFs are selected as an input into BPNN.

3. Evaluating each feature-subset solution (x_i) with BPNN model.

4. Updating individual solutions $F(x_i)$. The individual solution $F(x_i)$ is calculated based on the performance value of predicting cassava chips water content from the feature-subset (x_i) from the validation of MSE value.

5. Calculating the threshold value (d_g) of all neighbors in the search area by using the following formula of:

$$M = \left[M_{jk}\right] = \frac{\left\|F(x_j) - F(x_k)\right\|}{2} \tag{18}$$

$$d_g = median\left\{M_{jk} \in M : 1 \le j < k \le N_a\right\} \tag{19}$$

6. Repeating steps 6.1 to 6.4 for each x_i in stage 6.1. to 6.7 which are as follows:

6.1. Repairing the personal best solution (p_i) for each individual cockroach:

$$p_i \begin{cases} p_i = x_i & if\ F(x_i) < F(p_i) \\ p_i & otherwise \end{cases} \tag{20}$$

6.2. Calculating neighbors (N_i) from cockroaches i.

For k = 1 to N_a

$$N_i \begin{cases} N_i = N_i + 1 & if\ k : 1 \le k \le N_a, k \ne i\ AND\ M_{ik} < d_g \\ N_i & otherwise \end{cases} \tag{21}$$

6.3. Fixing darkest locations as the best solution in the group (l_i) based on:

$$l_i \begin{cases} l_i = l_{j_r} = \arg\min_k \left\{F(p_k)\right\}, k = \left\{i, j_r\right\} & if\ rand[0,1] < A_{\min\{N_i,3\}} \\ l_i & otherwise \end{cases} \tag{22}$$

where $\{i, j\}$ are two individuals who socialize cockroaches and p_k is the darkest location in each individual cockroach or referred to as the personal best.

6.4. Improving cockroach location (x_i):

$$x_i \begin{cases} x_i = C_o \oplus CR(C_o \oplus CR(w \oplus MT(x_i), p_i), l_i) & if\ hunger_i < t_{hunger} \\ x_i = random & otherwise \end{cases} \tag{23}$$

The fixed x_i value is influenced by three components, representing the velocity of the cockroach. MT represents the value of the mutation probability with variable w. If rnd random number [0, 1] is smaller than w value, one mutation process will be carried out. The second component is a cognitive component

in cockroaches that represents the thinking power of each cockroach. CR represents the crossover process between a_i and p_i with a probability value of C_o. Two-point crossover is selected randomly, where $point_1$ is $<point_2$, $point_1>1$ and $point_2<m$. The third component is $x_i = C_o \oplus CR(b_i, l_i)$, which is a social component of cockroach representing the power of collaboration in the *CR* group representing a crossover process between b_i and l_i with a probability value of C_o.

6.5. Correcting each feature-subset (x_i) with BPNN model.

6.6. Improving individual solutions $F(x_i)$ based on the value of the MSE validation with BPNN model.

6.7. Correcting values from $hunger_i$:

$$hunger_i = hunger_i + rand[0,1] * t_{hunger} \tag{24}$$

6.8. Improving the best solution T^{IB} for each iteration.

$$T^{IB} = \arg\max q(F(x_i)) \tag{25}$$

where the function $q(.)$ is the value of the solution for each cockroach.

7. Repairing the total best solution T^{TB} using iteration-best solution best T^{IB} with the formula:

$$T^{TB} \begin{cases} T^{TB} & if\ q(T^{TB}) \geq q(T^{IB}) \\ T^{IB} & otherwise \end{cases} \tag{26}$$

8. Improving the best feature-subset.

9. The iteration process will stop when the total-best solution T^{TB} has been reached and the best feature-subset has reached a predetermined iteration value.

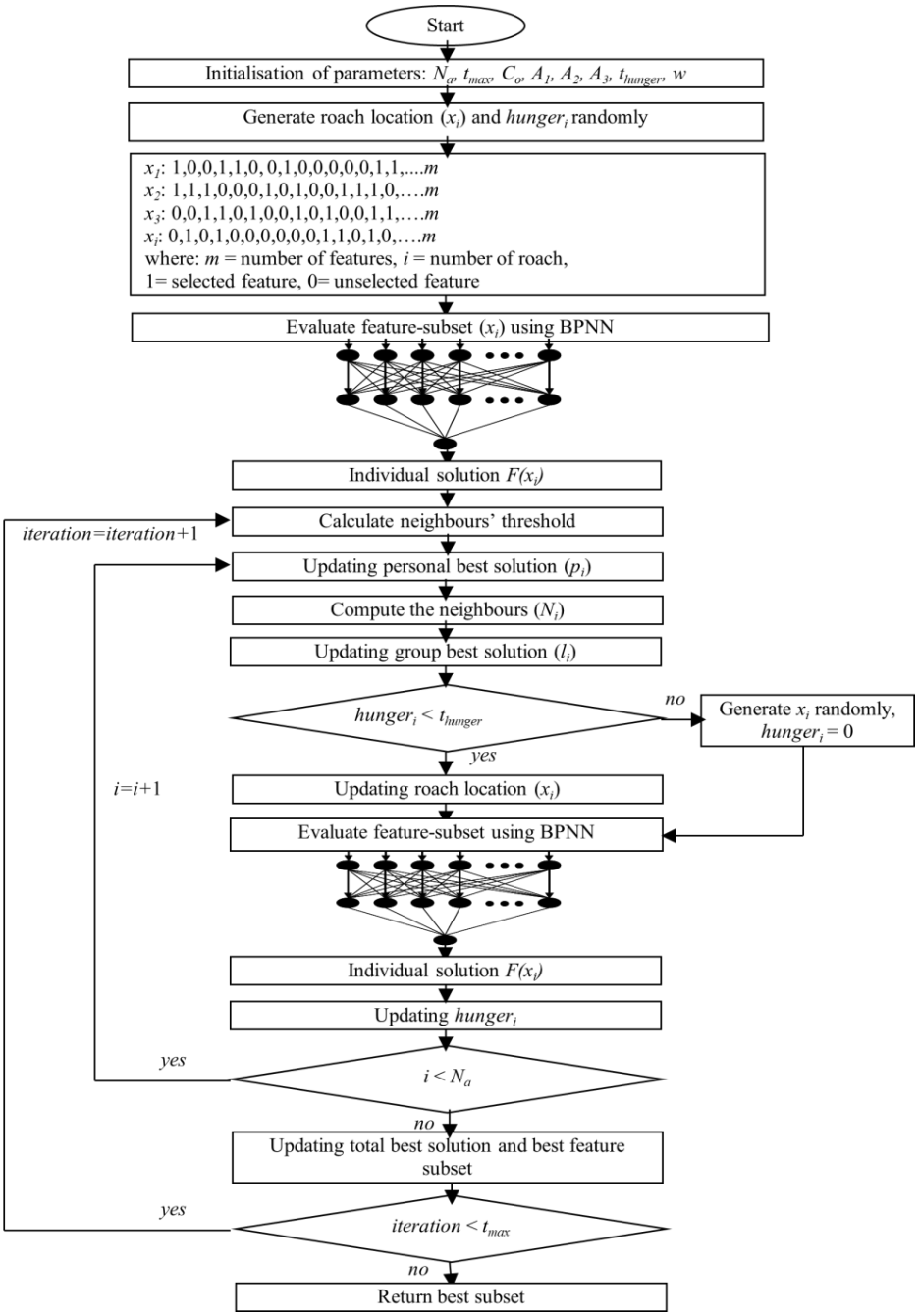

Fig. 2. Hybrid HRIO and ANN to predict the water content of cassava chips.

3 Results and Discussion

The principle of this research is that the external surface appearance of a food object caused by changes in the condition of its water content to be detected by using the computer vision method. This process includes water level detection in the process of drying cassava chips. The measurement of water content in cassava chips in this study utilized a wet base moisture content formula. Measuring the water content of cassava chips is performed at each level of dryness of the material according to three ranges of water content, which are: range 1 (wet) with water content of 55 - 70% wb, range 2 (semi-dry) with water content of 20 - 40% wb, and range 3 (optimal dryness) with a moisture content of 0 - 10% wb. Figure 3 depicts an example of a sample of cassava chips in various water content conditions in this study. Visually, it is hard to distinguish the level of dryness from each class of cassava chips (wet, semi-dry, and optimal dryness). Alternatively, a smart application with an intelligent system approach is required to solve this problem.

(a) (b) (c)

Fig. 3. The appearance of cassava chips during the drying process in various conditions of water content, such as: (a) wet / range 1; (b) semi-dry / range 2; (c) optimum dryness / range 3.

According to Harralick *et al.* [34], energy TFs are one parameter of gray level co-occurrence matrix (GLCM) which is used to measure the intensity of pixel pairs. The value of energy TFs will be even greater if the pixel value in digital images is more homogeneous. Figure 4a illustrates the image of cassava chips having a relatively similar energy to TFs pattern, indicating that the value of energy TFs from cassava chips in range 1 has the highest value with an average index value of all color spaces (0.223). It means that cassava chips in range 1 have high pixel of homogeneity. If the homogeneity of pixel pairs is higher, then the cassava chips texture in range 1 have a higher level of density and smoothness. Cassava chips in range 2 have low homogeneity with an average index value of all color spaces (0.081). This occurrence indicates that textures in range 2 began to be rougher and wrinkled because the chips had been dried for more than 140 minutes at 70 ºC, which also occurred in cassava chips at range 3. Figure 4b demonstrates that the entropy value of TFs in range 1 has a low value with an average index value for all color spaces (0.660). This appearance indicates that the texture of cassava chips at the beginning of the drying process is irregular and uneven; whereas in the range 2, the entropy value reaches the highest value with an average index value for all color spaces (0.829). Meanwhile, in range 3, the value of entropy TFs decreases along with the average index value for all color spaces (0.788). Based on observations using image analysis, it is concluded that longer dried cassava chips have a higher entropy TFs value. If cassava chips are at a maximum dry point, they absorb water in

relatively small amounts of water vapor in the drying chamber. Contrast TFs measure the level of variation is performed between pixels in a digital image. Figure 4c demonstrates that almost all contrast TFs have the same relative pattern except for $u_{(Luv)}$ and $v_{(Luv)}$ color spaces. This occurrence indicates that cassava chips in range 1 have contrast values with an average index for all color spaces (0.282), but gradually decrease to range 2 with an average index value for all color spaces (0.244). This result proves that cassava chips in range 2 have a variation of low gray degree differences. From the results of the image analysis, it is concluded that smaller amount of the water content in cassava chips produces higher contrast of TFs value. The homogeneity of TFs is tested to measure the level of closeness (bounding) of each element in the CCM. The homogeneity of TFs is expected to be higher if the gray level value for each pixel pair is relatively similar. Homogeneity of TFs will increase if the intensity variation in digital images decreases. Figure 4d indicates that almost all homogeneity of TFs has the same relative pattern except for $Y_{(CMYK)}$ and $u_{(Luv)}$. The value of cassava homogeneity chips in range 2 has a higher average value than in range 1. According to the average homogeneity of TFs, range 1 has a high value with an average index value for all color spaces of 0.442. This result proves that the gray degree value at each pixel is high, but the graph pattern slowly decreases when reaching range 2 where the average index value for all color spaces is 0.261. From range 2 to range 3, the chart pattern slowly decreases along with the average index value for all color spaces of 0.256. This result proves that the gray degree value continues to decrease when the drying process is completed, which affects the homogeneity value of TFs on cassava chips. Based on the results, longer drying process of cassava chips creates smaller homogeneity value of TFs. The inverse different moment (IDM) in TFs value indicates the smoothness of digital images based on the level of similarity in pixel pairs. The more homogeneous a digital image, IDM TFs value will be higher. IDM value is expected to be higher if the gray level at each pixel shows similarity. Figure 4e demonstrates that almost all IDM TFs have the same pattern except for $C_{(CMYK)}$. Cassava chips in range 1 have the lowest value compared to range 2 or range 3 with an average index value for all color spaces of 0.619. Cassava chips at range 2 water content have an average index value of 0.777 and slowly decline to range 3 with an average index value of 0.687. The decrease in this value indicates that the homogeneity of the image in range 2 is high, compared to range 1 and range 3. Thus, it can be concluded that higher water content of cassava chips leads to smaller IDM TFs value. Correlation of TFs signifies a linear dependency measure of the gray level of an image in a CCM. The correlation of TFs is expected to be higher if similar grayish pixel level has a high correlation. Figure 4f indicates that almost all values of correlation of TFs in range 1 have a low value with an average index value for all color spaces of 0.405. The chart pattern depicts higher trend in range 2 with an average index value for all color spaces of 0.510. By increasing the drying time, the TFs correlation also increases. In range 3, the value of the TFs correlation decreases along with the average index value for all color spaces of 0.476. The texture conditions of cassava chips that have been dried at high temperatures affect the color of the dried chips into dark colour due to the loss of water content. Therefore, it can be concluded that the lower the water content of cassava chips, the greater the value of the correlation of TFs. The sum mean TFs indicates the average grayish value of a digital image, which is expected to be higher if the mean grayish value of an image is also high. From the results of the sum mean of TFs, almost all TFs have different patterns

based on the condition of the cassava chips moisture content. Figure 4g indicates that the average sum mean value TFs in range 1 has a high value with an average index value for all color spaces of 0.438. This appearance is due to the high average value of grayish grades increasing in range 2 with an average index value for all color spaces of 0.447. Changes in texture value occur because the drying process is getting longer in range 2. The next graphic pattern tends to fall again in range 3 with an average index value for all color spaces of 0.399. This indicates that the gray level value in the image is getting lower. From the image analysis data, it is apparent that the lower the water content of cassava chips, the higher the sum mean value of TFs. Variance TFs indicate the value of element variations in the CCM. An image with a low grayish transition value will also have a low variance value. The variance value of TFs is expected to be greater if the grayish degree is spread evenly in the image. Figure 4h presents that almost all TFs have the same pattern except for $u_{(Luv).}$ The results of image analysis postulate that the average value of variance TFs in range 1 has an average index value for all color spaces of 0.311. This occurrence marks that the grayish degree of the image at the beginning of the drying process is in a homogeneous condition. Range 2 has a lower value with an average index value for all color spaces of 0.181. This occurrence clarifies that the value of variance TFs decreases. However, the pattern of variance TFs chart increases as the drying process progresses. The average index value for all color spaces in range 3 is 0.239. Thus, it is apparent that the higher the water content of cassava chips, the higher the value of variance TFs. Cluster tendency TFs indicate the level of grouping in each pixel of similar gray image. Figure 4i indicates that almost all cluster tendency TFs have similar pattern except for $v_{(Luv).}$ It is apparent that the highest value is reached in range 1 with an average index value for all color spaces of 0.320, then this value drops in range 2 by 0.187. Furthermore, in range 3, the value of cluster tendency TFs rises again to 0.257, indicating that if the water content of cassava chips is low, the cluster tendency TFs are also lower. The maximum probability of TFs presents the highest number of pixel pair intensity values in the CCM. The maximum probability TFs also measures the regularity of pixels in a digital image. It is concluded that the higher the maximum probability TFs, the higher the order level. Figure 4j indicates that almost all maximum probability TFs have similar patter except for $C_{(CMYK)}$. This can be explained that the maximum probability TFs in range 1 has a high value with an average index value for all color spaces of 0.302. This appearance indicates that in range 1, the texture of cassava chips has a high level of regularity. However, in the range 2 the maximum probability TFs value decreases along with the average index value for all color spaces by 0.147 and rises again in range 3 with an average index value for all color spaces of 0.193. Therefore, it is obvious that the lower the water content of cassava chips, the maximum probability TFs value will be lower.

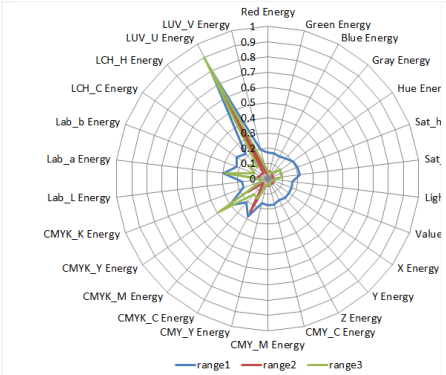
Red Energy
Green Energy
Blue Energy
Gray Energy
Hue Ener
Sat_h
Sat
Ligh
Value
X Energy
Y Energy
Z Energy
CMY_C Energy
CMY_M Energy
CMY_Y Energy
CMYK_C Energy
CMYK_M Energy
CMYK_Y Energy
CMYK_K Energy
Lab_L Energy
Lab_a Energy
Lab_b Energy
LCH_C Energy
LCH_H Energy
LUV_U Energy
LUV_V Energy
range1
range2
range3

(a)

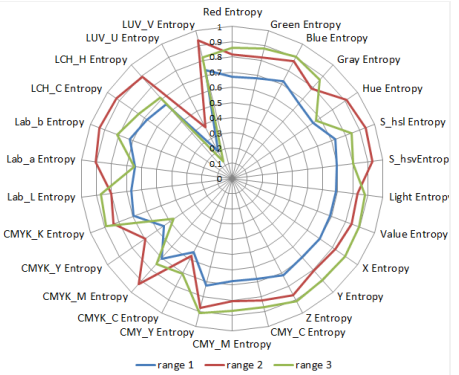
Red Entropy
Green Entropy
Blue Entropy
Gray Entropy
Hue Entropy
S_hsl Entropy
S_hsvEntrop
Light Entropy
Value Entropy
X Entropy
Y Entropy
Z Entropy
CMY_C Entropy
CMY_M Entropy
CMY_Y Entropy
CMYK_C Entropy
CMYK_M Entropy
CMYK_Y Entropy
CMYK_K Entropy
Lab_L Entropy
Lab_a Entropy
Lab_b Entropy
LCH_C Entropy
LCH_H Entropy
LUV_U Entropy
LUV_V Entropy
range 1
range 2
range 3

(b)

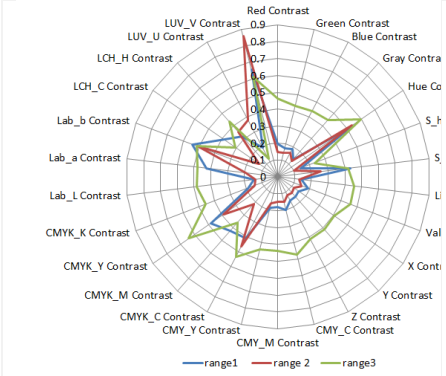
Red Contrast
Green Contrast
Blue Contrast
Gray Contra
Hue Co
Val
X Conti
Y Contrast
Z Contrast
CMY_C Contrast
CMY_M Contrast
CMY_Y Contrast
CMYK_C Contrast
CMYK_M Contrast
CMYK_Y Contrast
CMYK_K Contrast
Lab_L Contrast
Lab_a Contrast
Lab_b Contrast
LCH_C Contrast
LCH_H Contrast
LUV_U Contrast
LUV_V Contrast
range1
range 2
range3

(c)

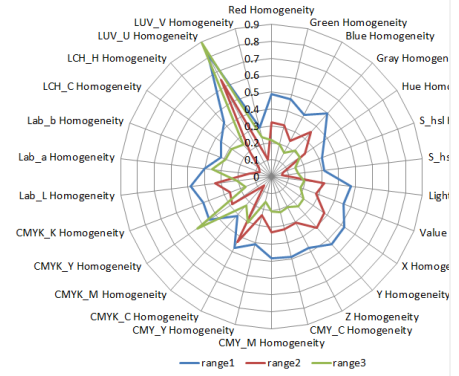
Red Homogeneity
Green Homogeneity
Blue Homogeneity
Gray Homogen
Hue Homo
Value
X Homoge
Y Homogeneity
Z Homogeneity
CMY_C Homogeneity
CMY_M Homogeneity
CMY_Y Homogeneity
CMYK_C Homogeneity
CMYK_M Homogeneity
CMYK_Y Homogeneity
CMYK_K Homogeneity
Lab_L Homogeneity
Lab_a Homogeneity
Lab_b Homogeneity
LCH_C Homogeneity
LCH_H Homogeneity
LUV_U Homogeneity
LUV_V Homogeneity
range1
range2
range3

(d)

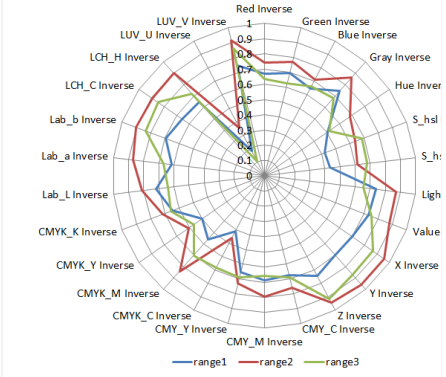
Red Inverse
Green Inverse
Blue Inverse
Gray Inverse
Hue Inver
S_hsl
Ligh
Value
X Inverse
Y Inverse
Z Inverse
CMY_C Inverse
CMY_M Inverse
CMY_Y Inverse
CMYK_C Inverse
CMYK_M Inverse
CMYK_Y Inverse
CMYK_K Inverse
Lab_L Inverse
Lab_a Inverse
Lab_b Inverse
LCH_C Inverse
LCH_H Inverse
LUV_U Inverse
LUV_V Inverse
range1
range2
range3

(e)

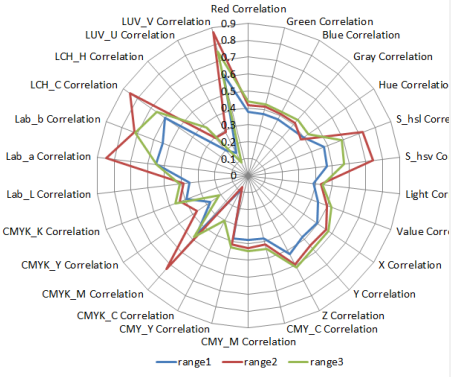
Red Correlation
Green Correlation
Blue Correlation
Gray Correlation
Hue Correlatio
S_hsl Corre
S_hsv Co
Light Cor
Value Corr
X Correlation
Y Correlation
Z Correlation
CMY_C Correlation
CMY_M Correlation
CMY_Y Correlation
CMYK_C Correlation
CMYK_M Correlation
CMYK_Y Correlation
CMYK_K Correlation
Lab_L Correlation
Lab_a Correlation
Lab_b Correlation
LCH_C Correlation
LCH_H Correlation
LUV_U Correlation
LUV_V Correlation
range1
range2
range3

(f)

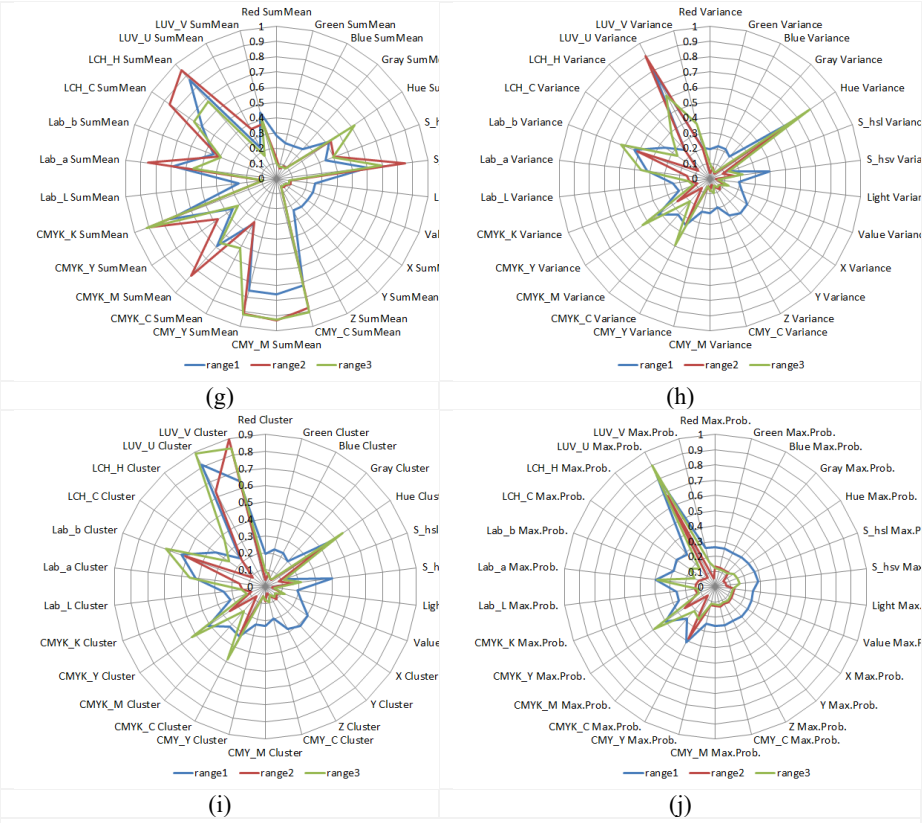

Fig. 4. Distribution graphs normalized TFs from cassava chips at various levels of drying.

Figures 5 present a sensitivity analysis based on the MSE value of validation data to predict the water content of cassava chips during drying with several learning rates, such as: 0.1, 0.5, and 0.9, and momentum values of 0.1, 0.5, and 0.9. Figure 5a presents the lowest MSE validation value achieved by feature-subset $Z_{(XYZ)}$ TFs with MSE value of 0.000129 by using learning rate of 0.5 and momentum of 0.5. Figure 5b depicts the lowest MSE value achieved by the energy TFs feature subset utilizing all color spaces with an MSE value of 0.000104 by using a learning rate of 0.1 and momentum of 0.9. Therefore, the feature subset of the energy in TFs using all color spaces has the best performance as an ANN input to predict output, including the water content of cassava chips during the drying process. Figure 6a presents the results of the plot of optimization of normalized MOO fitness values by using the HRIO method, indicating effective performance as long as the objective function value decreases until it converges during the iteration process. Figure 6b depicts the performance of the training process by using BPNN with the feature subset obtained from the HRIO method. BPNN training results have effective performance as long as the value of MSE training continues to decline and converge as the number of iterations increases. The prediction model built with ANN by using a selection feature with the HRIO optimization method produces a lower MSE value compared to the ANN prediction model without using feature selection.

ANN modeling results using HRIO optimization indicate the lowest MSE value in training data with a value of 0.000056 and the lowest MSE value in the data validation is 0.000098. Figure 7 indicates the relationship between real data and predicted data. The value of R^2 (0.98) indicates significant results by using a combination of ANN modeling and HRIO optimization models to predict the water content of cassava chips during the drying process. Table 1 depicts the optimum weights results from the input layer to the hidden layer obtained from BPNN model. Table 2 presents the optimum weights results from the hidden layer to the output layer from BPNN model. The structure of the ANN model is depicted in Figure 8.

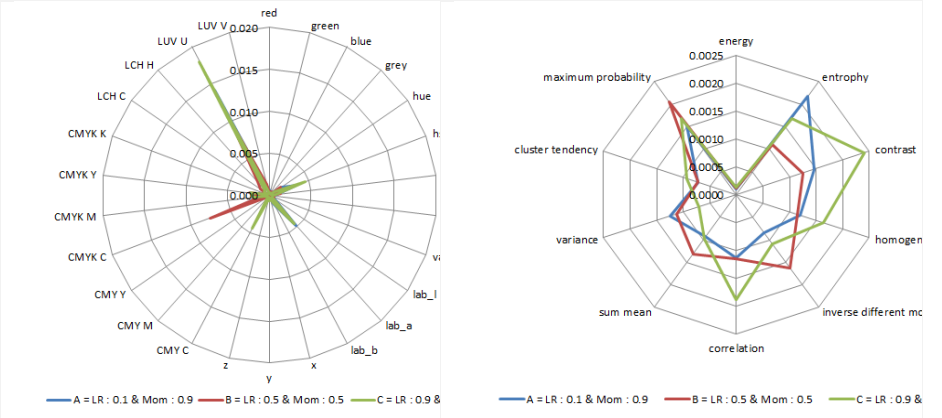

(a) (b)

Fig. 5. Sensitivity analysis feature-subset TFs on various color spaces and TFs based on the validation MSE value using various combinations of learning rate (LR) and momentum (mom).

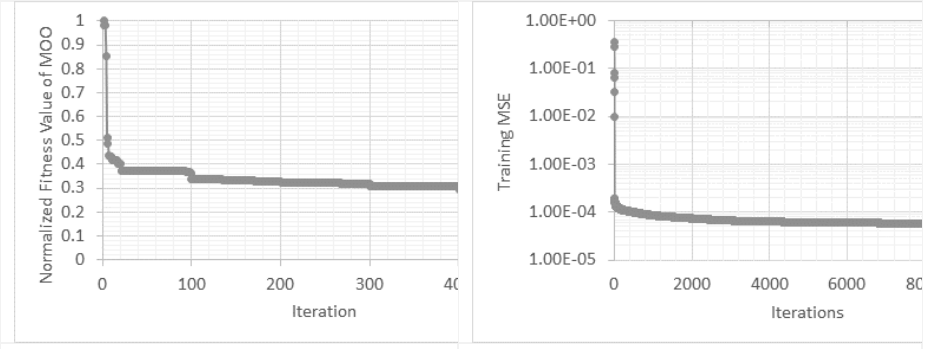

(a) (b)

Fig. 6. Plot of the best MOO fitness value and Performance of BPNN training process.

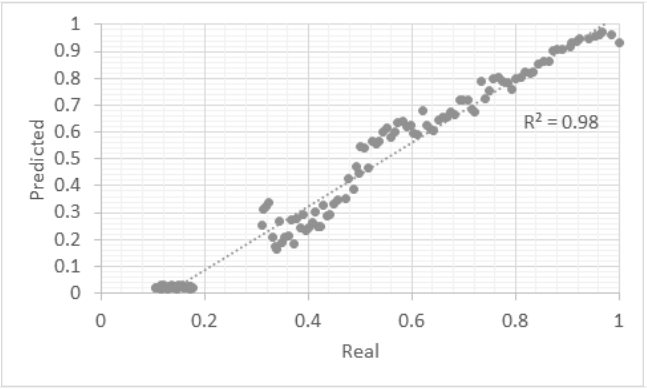

Fig. 7. Relations between real-predicted data.

Table 1. The weights from the input layer to the hidden layer.

V(x,y)		x					
		1	2	3	4	5	6
y	1	-0.855	0.269	-0.426	-1.112	-0.819	-3.283
	2	-2.118	1.007	3.164	1.60E+00	1.189	-11.458
	3	-12.036	-4.580	1.704	3.288	-3.082	-5.305
	4	-2.763	2.210	-1.795	-2.083	8.80E+00	1.519
	5	3.472	-7.73E-01	-0.166	-0.361	-1.071	1.667
	6	-8.826	3.63E+00	-1.973	-0.865	-1.926	5.803
	7	2.144	0.935	-8.54E-01	1.204	-3.088	-1.162
	8	-7.01E+00	-3.952	5.684	-1.738	-4.999	-4.866
	9	11.615	6.148	-5.402	-3.179	2.812	10.796
	10	1.016	-0.365	-0.644	-2.279	-0.863	-4.768

Table 2. The weights from the hidden layer to the output layer.

Weights									
W1	W2	W3	W4	W5	W6	W7	W8	W9	W10
-3.696	-6.344	-9.967	-6.247	2.8 11	-6.895	2.3 30	-6.029	11.3 43	-4.345

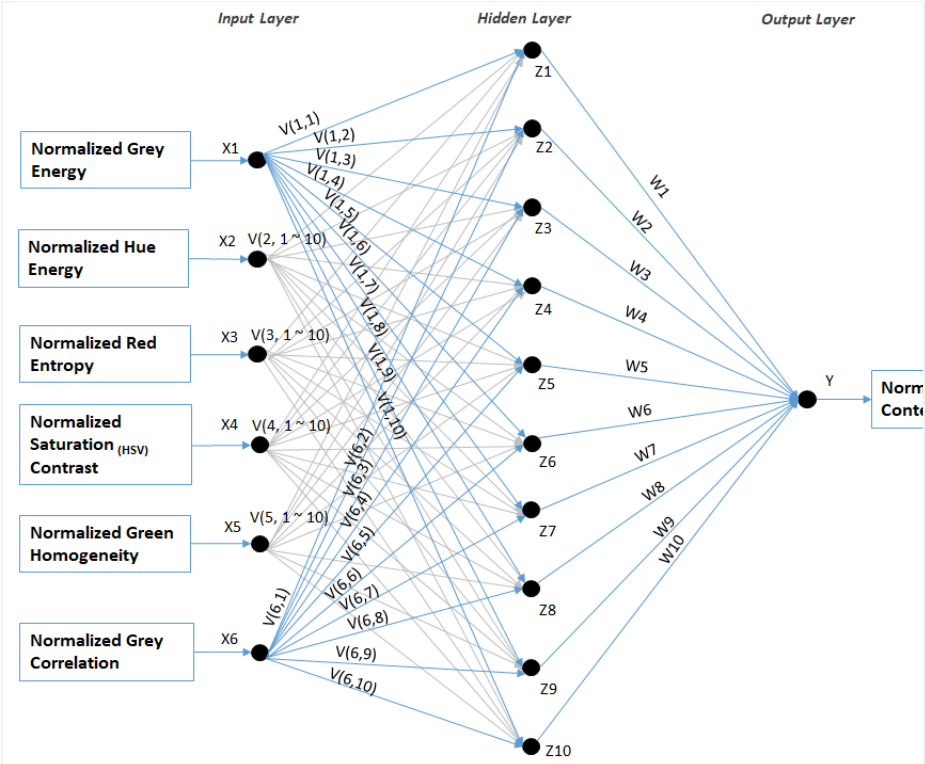

Fig. 8. ANN model for monitoring the water content of cassava chips during drying process.

4 Conclusion

In this study, textural features (TFs) were extracted from various color spaces such as grey, RGB, HSV, HSL, Lab, XYZ, LCH, Luv, CMY, and CMYK to model the water content of cassava chips during the drying process. Back-propagation neural network (BPNN) has been successfully tested to model the relationship between TFs and cassava chip water content. Based on the results of the test, the feature subset of the energy TFs using various color spaces indicates the best performance compared to other various features subset without using the feature selection method. The feature selection method has been proven to be successful in improving the predictive performance of artificial neural network (ANN). In overall, there is a significant difference between the ANN model using the feature selection and the ANN model that was built without feature selection. Based on the results of the optimization, the hungry roach infestation optimization (HRIO) method achieves the best performance to optimize fitness values by using multi-objective optimization (MOO) to minimize prediction errors and number of feature subset. From the ANN modeling results with HRIO optimization, mean square error (MSE) value in the training data is 0.000056 and the MSE value in the data validation is 0.000098 with R^2 values between the real-predicted data of 0.98. ANN

model obtained in this study is applicable to monitor the drying process of cassava chips in real-time during the drying process to get the best moisture content.

Acknowledgements

The authors wish to acknowledge support and funding from the Professor Research Grants Program, Universitas Brawijaya.

References

1. Dudu, O.E., Oyedeji, A.B., Oyeyinka, S.A., Ma, Y.: Impact of Steam-Heat-Moisture Treatment on Structural and Functional Properties of Cassava Flour and Starch. Int. J. Biol. Macromol 126, 1056-1064 (2019).
2. Liu, R., Sun, W., Zhang, Y., Huang, Z., Hu, H., Zhao, M.: Preparation of Starch Dough Using Damage Cassava Starch Induced by Mechanical Activation to Develop Staple Foods: Application in Crackers. Food Chem. 271, 284-290 (2019).
3. Jensen, S., Skibsted, L.H., Kidmose, U., Thybo, A.K.: Addition of Cassava Flours in Bread Making: Sensory and Textural Evaluation. LWT - Food Sci. Technol. 60(1), 292-299 (2015).
4. Barzegar, M., Zare, D., Stroshine, R.L.: An Integrated Energy and Quality to Optimization of Green Peas Drying in A Hot Air Infrared-Assisted Vibratory Bed Dryer. J. Food Eng. 166, 302-315 (2015).
5. Kumar, V., Sharma, H.K., Singh, K.: Effect of Precooking on Drying Kinetics of Taro (*Colocasia esculenta*) Slices and Quality of Its Flour. Food Biosci. 20, 178-186 (2017).
6. Hadawey, A., Tassou, S.A., Chaer, I., Sundarajan, R.: Unwrapped Food Product Display Shelf Life Assessment. Energy Procedia 123, 62-29 (2017)
7. Ali, B.N., Oummadi, S., Portuguez, E., Alzina, A., Smith, D.S.: Thermal Conductivity of Ceramic Green Bodies During Drying. J. Eur. Ceram. Soc. 37(4), 1839-1846 (2017).
8. Hossain, S.M.Z., Mansour, N., Sultana, N.: Design of A Laboratory Experiment for The Performance Analysis of A Retrofitted Tray Dryer Unit. Educ. Chem. Eng. 18, 35-44 (2017).
9. Aviara, N.A., Onuoha, L.N., Falola, O.E., Igbeka, J.C.: Energy and Exergy Analysis of Native Cassava Starch Drying in A Tray Dryer. Energy 73, 809-817 (2014).
10. Aghbashlo, M., Hosseinpour, S., Ghasemi-Varnamkhasti, M.: Computer Vision Technology for Real Time Food Quality Assurance During Drying Process. Trends Food Sci. Technol. 39, 76-84 (2014).
11. Dutta, M.K., Singh, A., Ghosal, S.: A Computer Vision Based Technique for Identification of Acrylamide in Potato Chips. Comput. Electron. Agric. 119, 40-50 (2015).
12. Baigvand, M., Banakar, A., Minaei, S., Khodaei, J., Khazaei, N.B.: Machine Vision System for Grading of Dried Figs. Comput. Electron. Agric. 119, 158-165 (2015).
13. Benalia, S., Cubero, S., Montalban, J.M.P., Bernardi, B., Zimbalatti, G., Blasco, J.: Computer Vision for Automatic Quality Inspection of Dried Figs (*Ficus carica* L.) in Real Time. Comput. Electron. Agric. 120, 17-25 (2015).
14. Romani, S., Rocculi, P., Mendoza, F., Rosa, M.D.: Image Characterization of Potato Chip Appearance During Frying. J. Food Eng. 93, 487-494 (2009).
15. Yadollahinia, A., Jahangiri, M.: Shrinkage of Potato Slice During Drying. J. Food Eng. 94, 52-58 (2009).

16. Huang, Y., Lan, Y., Thomson, S.J., Fang, A., Hoffmann, W.C., Lacey, R.E.: Development of Soft Computing and Applications in Agricultural and Biological Engineering. Comput. Electron. Agric. 71, 107-127 (2010).
17. Khazaei, N.B., Tavakoli, T., Ghassemian, H., Khoshtaghaza, M.H., Banakar, A.: Applied Machine Vision and Artificial Neural Network for Modeling and Controlling of the Grape Drying Process. Comput. Electron. Agric. 98, 205-213 (2013).
18. Ni, H., Gunasekaran, S.: Food Quality Prediction with Neural Networks. Food Technol. 52, 60-65 (1998).
19. Xie, G., Xiong, R.: Use of Hyperbolic and Neural Network Models in Modelling Quality Changes of Dry Peas in Long Time Cooking. J. Food Eng. 41, 151-162 (1999).
20. Singh, R.R.B., Ruhil, A.P., Jain, D.K., Patel, A.A., Patil, G.R.: Prediction of Sensory Quality of UHT Milk – A Comparison of Kinetic and Neural Network Approaches. J. Food Eng. 92, 146-151 (2009).
21. Azadbakht, M., Aghili, H., Ziaratban, A., Torshizi, M.V.: Application of Artificial Neural Network Method to Exergy and Energy Analysis of Fluidized Bed Dryer for Potato Cubes. Energy 120, 947-958 (2017).
22. Wu, J., Yang, S.X., Tian, F.: A Novel Intelligent Control System for Flue-Curing Barns Based on Real Time Image Features. Biosyst. Eng. 123, 77-90 (2014).
23. Gheyas, I.A., Smith, L.S.: Feature Subset Selection in Large Dimensionality Domains. Pattern Recognit. 43, 5-13 (2010).
24. Hendrawan, Y. and Murase, H.: Neural-Genetic Algorithm as Feature Selection Technique for Determining Sunagoke Moss Water Content. Eng. Agric. Environ. Food. 3(1), 25-31 (2010).
25. Hendrawan, Y. and Murase, H.: Non-destructive Sensing for Determining Sunagoke Moss Water Content: Bio-inspired Approaches. Agric. Eng. Int.: CIGR J. 13(1), 1564. (2011a).
26. Hendrawan, Y. and Murase, H.: Bio-Inspired Feature Selection to Select Informative Image Features for Determining Water Content of Cultured Sunagoke Moss. Expert Syst. Appl. 38(11), 14321-14335 (2011b).
27. Hendrawan, Y. and Murase, H.: Neural-Intelligent Water Drops Algorithm to Select Relevant Textural Features for Developing Precision Irrigation System Using Machine Vision. Comput. Electron. Agric. 77(2), 214-228 (2011c).
28. Hendrawan, Y. and Murase, H.: Precision irrigation for Sunagoke moss production using intelligent image analysis. Environ. Control. Biol. 49(1), 1-21 (2011d).
29. Hendrawan, Y. and Al Riza, D.F.: Machine Vision Optimization Using Nature–Inspired Algorithms to Model Sunagoke Moss Water Status. Int. J. Adv. Sci. Eng. Inf. Technol. 6, 2088-5334 (2016).
30. Ondimu, S.S. and Murase, H.: Comparison of Plant Water Stress Detection Ability of Colour and Gray-Level Texture in Sunagoke Moss. Trans. ASABE 51(3), 1111-1120 (2008).
31. Kopparapu, S.K.: Lighting Design for Machine Vision Application. Image Vis. Comput. 24, 720-726 (2006).
32. Handl, J., Douglas, B. K., Knowles, J.: Multiobjective Optimization in Bioinformatics and Computational Biology. IEEE/ACM Transactions on Computational Biology and Bioinformatics 4(2), April-June (2007).
33. Hendrawan, Y. and Murase, H.: Precision irrigation for Sunagoke moss production using intelligent image analysis. Environ. Control. Biol.47(1), 21-36 (2009).
34. Haralick, R. M., Shanmugam, K., Its'hak Dinstein.: Textural Features for Image Classification. IEEE Transaction on Systems, Man, and Cybernetics 3(6): 610-621, (1973).
35. Rotterman, Y. and Porat, M.: Colour Image Coding Using Regional Correlation of Primary Colours. Image Vis. Comput. 25, 637-651 (2006).
36. Angulo, J. and Serra, J.: Modelling and Segmentation of Colour Images in Polar Representations. Image Vis. Comput. 25, 475-495 (2007).

37. Leon, K., Mery, D., Pedreschi, F., Leon, F.: Colour Measurement in L*a*b* Units from RGB Digital Images. Food Res. Int. 39, 1084-1091 (2006).
38. Kim, M.C.: Comparative Colour Gamut Analysis of xvYCC Standard. Displays 29, 376-385 (2008).
39. Palm, C.: Colour Texture Classification by Integrative Co-Occurrence Matrices. Pattern Recognit. 37, 965-976 (2004).
40. Pydipati, R., Burks, T. F., Lee, W. S.: Identification of Citrus Disease Using Colour Texture Features and Discriminant Analysis. Comput. Electron. Agric. 52, 49-59 (2006).
41. Havens, T. C., Spain, C. J., Salmon, N. G., Keller, M.: Roach Infestation Optimization. IEEE Swarm Intelligence Symposium St. Louis MO USA, September 21-23 (2008).
42. Jeanson, R., Rivault, C., Deneubourg, J.L., Blanco, S., Fourniers, R., Jost, C., Theraulaz, G.: Self-organized aggregation in cockroaches. J. Anim. Behav. 69, 169-180 (2005).